Experimental observation of ion beams in the Madison Helicon eXperiment

Matt Wiebold, Yung-Ta Sung, and John E. Scharer
Electrical and Computer Engineering, University of Wisconsin—Madison, Madison, Wisconsin 53706, USA

(Received 10 March 2011; accepted 1 May 2011; published online 13 June 2011)

Argon ion beams up to $E_b = 165$ eV at $P_{rf} = 500$ W are observed in the Madison Helicon eXperiment (MadHeX) helicon source with a magnetic nozzle. A two-grid retarding potential analyzer (RPA) is used to measure the ion energy distribution, and emissive and rf-filtered Langmuir probes measure the plasma potential, electron density, and temperature. The supersonic ion beam ($M = v_i/c_s$ up to 5) forms over tens of Debye lengths and extends spatially for a few ion-neutral charge-exchange mean free paths. The parametric variation of the ion beam energy is explored, including flow rate, rf power, and magnetic field dependence. The beam energy is equal to the difference in plasma potentials in the Pyrex chamber and the grounded expansion chamber. The plasma potential in the expansion chamber remains near the predicted $eV_p \sim 5kT_e$ for argon, but the upstream potential is much higher, likely due to wall charging, resulting in accelerated ion beam energies $E_b = e[V_{beam} - V_{plasma}] > 10kT_e$. © *2011 American Institute of Physics*. [doi:10.1063/1.3596537]

I. INTRODUCTION

Helicon plasma sources, known for their efficient plasma production, have been investigated for use in space propulsion systems for some time. Several groups have observed accelerated ion populations in these sources, particularly with a physical and/or magnetic field expansion region.[1–12]

Double layers (DLs) are narrow (tens of Debye lengths) regions of positive and negative charge separated in space. They provide a transition region between two quasi-neutral plasmas with different properties, such as density or temperature. DLs have been studied extensively in several types of sources, and several reviews are present in the literature.[13–15] Recently, current-free double layers (CFDLs) have been observed in an expanding magnetic field in several helicon sources.[1–12] These double layers form without a net current through the DL.[16–18] Ions traverse the potential structure of the double layer and gain directed energy, and there has been interest in using this directed ion flux as a source of thrust.

Charles[2–5] was one of the first to observe a current-free double layer in an expanding helicon source with an energy analyzer using their *Chi-Kung* device. *Chi-Kung* consists of a 20 cm long double-saddle antenna, driven at 13.56 MHz, wrapped around a 15 cm diameter, 30 cm long glass tube, which is connected to a 32 cm diameter grounded diffusion chamber. Two solenoids provide a magnetic field up to 250 G. Beam energies up to $E_b = 3kT_e$, or 25 eV, were observed at argon pressures below 0.5 mTorr, which formed over ~50 Debye lengths. Higher upstream electron temperatures were observed upstream of the double layer.

Cohen reported ion acceleration up to 30 eV ($4kT_e$) initially[1] and later[19] to 65 eV ($3–10kT_e$) in argon using laser induced fluorescence (LIF) in their Magnetic Nozzle Experiment (MNX) *MNX* helicon device with a magnetic nozzle. *MNX* consists of a 4 cm diameter double-saddle antenna, driven at 26.75 MHz, wrapped around the 30 cm long glass source tube, which is attached to a 20 cm diameter, 45 cm long main chamber. A 1 cm diameter metal aperture separates the main chamber and the 10 cm diameter, 1 m long expansion region (ER), which leads to a drift chamber. Differential pumping and the low conductance aperture provide a large pressure differential (up to a factor of 10) between the main chamber and the ER. Two solenoids and a nozzle coil coincident with the aperture provide a magnetic field of several hundred G with an adjustable peak field up to 1.4 kG. Typical conditions are $P_{rf} \sim 500$ W, $B \sim 575$ G with a 1.4 kG nozzle peak, and pressures of 0.5 mTorr in the main chamber and 0.135 mTorr in the ER. They concluded the ion acceleration is not due to magnetic nozzle acceleration or simple plasma expansion but is due to a double layer that is induced near the aperture. They also saw evidence[19] of a two-temperature electron distribution downstream of the ion acceleration, with higher tail electron temperatures (0.1% fast electrons), which they claimed may be responsible for the higher potential drops (and beam energies) in their system.

Sutherland[20] observed double layer formation in the large-volume *WOMBAT* helicon reactor, up to $E_b = 5–7kT_e$ in argon. The reactor consists of a 50 cm long, 20 cm diameter Pyrex tube joined to a 1 m diameter grounded diffusion chamber. Up to 500 W of 7.2 MHz rf power is fed into the double-saddle antenna, and a magnetic field of 250 G is provided by two solenoids. The ion beam forms over ~20 Debye lengths at argon pressures between 0.09 and 0.3 mTorr, and the DL location was found to be tied to the magnetic field profile, not the location of the physical expansion.

Experiments on the *HELIX/LEIA* device at West Virginia University have investigated the time development of the double layer as well as the effect of rf frequency using LIF and energy analyzers.[6,11,21] The *HELIX/LEIA* device

consists of a 10 cm diameter, 61 cm long Pyrex tube connected to a 15 cm diameter, 91 cm long grounded chamber, which is then connected to a 2 m diameter, 4.5 m long space chamber. Rf power up to 2 kW is coupled to a 19 cm long half-turn double-helix antenna wrapped around the Pyrex tube, and argon pressures are 0.2 mTorr in the source and 0.05 mTorr in the space chamber. Double layer and ion beam formation were observed at rf frequencies above 11.5 MHz, with ion beam energies around 15 eV and spatial extents of tens of Debye lengths; however, formation over hundreds of Debye lengths has also been observed on a variant of this system.[6] They measured low frequency (ion acoustic) instabilities at rf frequencies below 11.5 MHz, which they indicate to prevent the DL from forming below the threshold frequency.

Lafleur *et al.*[22] measured the plasma potential with a 4-grid retarding potential analyzer (RPA) and an emissive probe (EP) in their *Piglet* helicon reactor, which consists of an 18 cm long, 13.6 cm inner diameter Pyrex tube connected to a 28.8 cm long, 30 cm diameter aluminum diffusion chamber with a static, expanding magnetic field of 160 G (maximum). An ion beam with energy $E_b \sim 18$ eV was observed, accelerating over 15 cm, at a pressure of 0.33 mTorr with a double saddle coil antenna at 200 W rf power and 13.56 MHz. The electron temperature $kT_e \sim 5$ eV at 0.33 mTorr is measured downstream of the acceleration region using an rf-compensated Langmuir probe (LP). Their group also measured beams present in their reactor only for a narrow range of magnetic fields (10–30 G), where a large density peak was observed (up to 1.5×10^{11} cm^{-3}) at low magnetic fields (~20 G).[23,24]

Recently, Virko *et al.*,[9] using RPAs, observed ion beams in argon accelerated over several centimeters with energies ($E_b = e[V_{beam} - V_{plasma}]$) approaching 75 eV in their 4.5 cm diameter quartz helicon system with fixed permanent magnets. With an axially monotonic magnetic field profile with argon pressures below 1 mTorr, intense pumping was required to achieve ambipolar ion acceleration up to 55 eV, which occurred even at zero magnetic field. With a magnetic cusp, they found that the insulation of high-density source and low-density drift regions created by the cusp led to non-ambipolar ion acceleration due to an extended potential drop (DL) between the two regions, over 5–6 cm. Ion energies up to 75 eV were observed in this case at 700 W rf power and at pressures near 0.1 mTorr. Emissive probes were used to measure plasma potentials, from 75 V to 110 V, in the source region.

Takahashi[25–27] has observed ion beam formation in argon in the *EMPI* device as well as the *Chi-Kung* device at ANU used by Charles.[2–5] The *EMPI* device, similar to the *Chi-Kung* device, consists of an insulating source tube, 30 cm long, and a 20.8 cm diameter grounded diffusion chamber. A triple-turn loop antenna driven at 13.56 MHz is wrapped around the source tube and up to 200 W rf power is supplied. Typical conditions for beam formation are pressures $p_{Ar} \sim 0.4$–0.6 mTorr, $P_{rf} \sim 200$ W, and $B \sim 200$–400 G. By testing different source tube diameters, they found that when the argon ions become magnetized in the source region, the DL and ion beam form. Two-temperature electron distributions were also measured on these devices, with lower tail than bulk electron temperatures.

Fredriksen *et al.*[10] and Byhring *et al.*[8] have carried out ion beam formation experiments in argon in the *Njord* double-saddle rf device of 13.7 cm diameter with source-region plasma potentials around 50 V. They have observed beams of 34–40 eV energy with an 8% beam fraction at low flow rates (1.2–1.5 sccm) utilizing an RPA, with 400–600 W of rf power and magnetic fields in the 110–250 G range. They indicate a current free double layer forms 10 cm downstream from the maximum magnetic field gradient in the expansion region. They also added a magnetic coil in the spherical dome region to extend the magnetic field expansion and observed 25 eV argon ion beams which disappear when the extra coil current is high enough such that the plasma is well confined into the downstream region, and the potential drop vanishes.

Previous research on the Madison Helicon eXperiment (MadHeX) experiment has explored neutral depletion[28] and bulk plasma acceleration (to ~1 km/s) at high rf powers (500 W-3 kW) and high ionization levels (96%) at higher gas pressures (1–10 mTorr Ar) and flow rates (18–150 sccm) in a nozzle magnetic field. Tysk[29] utilized this facility without the expansion chamber with a uniform magnetic field at higher pressures (3 mTorr) and powers (800 W) to investigate the variation of radial density and electron temperature profiles with magnetic field. Good agreement was found between measured and modeled helicon wave phase velocities. In the current work, we present results of ion beam acceleration at lower pressures (<1 mTorr) and flow rates (<10 sccm) in the MadHeX helicon system incorporating a nozzle magnetic field and expansion chamber. We have observed argon ion beam energies up to 165 eV at 500 W coupled rf power, and we examine the effects of flow rate, magnetic field strength, and rf power on ion beam acceleration, plasma density, electron temperature, and plasma potential.

Section II describes the MadHeX experimental system. Section III describes the diagnostics used, including the RPAs and probes. Section IV presents the results, and Sec. V includes a discussion and interpretation of the results.

II. EXPERIMENTAL APPARATUS

The MadHeX (Ref. 28) (shown in Fig. 1) device consists of a 10 cm inner-diameter (ID) Pyrex tube, 1.5 m long, joined with a grounded, stainless steel expansion chamber, 45 cm in diameter and 70 cm long. Steel mesh (18 cm diameter) surrounds the Pyrex chamber and is electrically grounded to the expansion chamber. Argon gas flows into the Pyrex tube through a 5 mm ID copper tube through the left (upstream) aluminum endplate, which is electrically grounded to the steel mesh. An 8-in. Varian turbo-molecular pump (550 L/s on N_2) is located at the bottom of the expansion chamber (downstream). MKS 910 DualTrans piezoelectric + Pirani gauges located at the upstream and downstream endplates measure the pressure at these locations, which are shown in Fig. 2. A Bayard-Alpert ionization gauge measures the base pressure of the system, typically

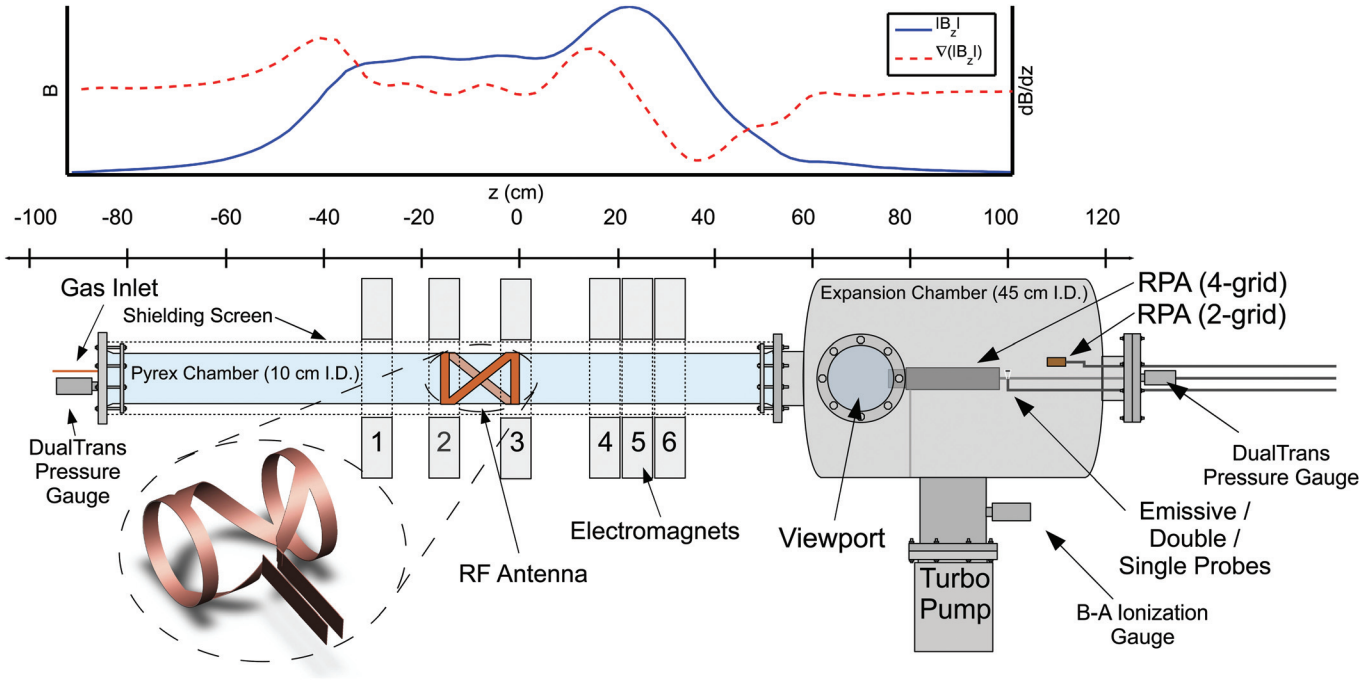

FIG. 1. (Color online) MadHeX helicon facility. The rf antenna is shown in the lower left corner and the static magnetic field value and gradient are shown above the system.

less than 10^{-6} Torr. A half-turn, double-helix antenna, 18 cm long and 13 cm in diameter (pictured in the inset of Fig. 1) surrounds the Pyrex chamber. The downstream edge of the antenna denotes $z = 0$ cm in the system. Positive z is in the direction of the gas flow, from upstream to downstream.

The axial magnetic field is provided by six electromagnets, each 7 cm wide with an 18 cm bore. The magnetic field profile is configured in a "nozzle" profile with a mirror ratio $R_m = 1.44$ with the peak at $z = 28$ cm. A Sorensen DC power supply provides up to 180 A, which corresponds to a field of up to 1.04 kG in the source region. The on-axis B field (B_z) value and gradient are shown in Fig. 3 for a magnet current of 60 A. Magnetic field values given below without a specified z position refer to the magnetic field value in the antenna region from $z = 0$ to $z = -18$ cm.

Rf power at 13.56 MHz is provided by an HP 33120A function generator, which is then fed to a Comdel CX10KS amplifier, capable of delivering up to 10 kW steady-state. A two-capacitor matching network is used to match to the antenna impedance, and forward and reflected powers are measured with a Connecticut Microwave directional coupler with calibrated rf diodes. The matchbox is tuned to reduce the steady-state reflected power to below 5% of the incident power in steady-state for all cases shown.

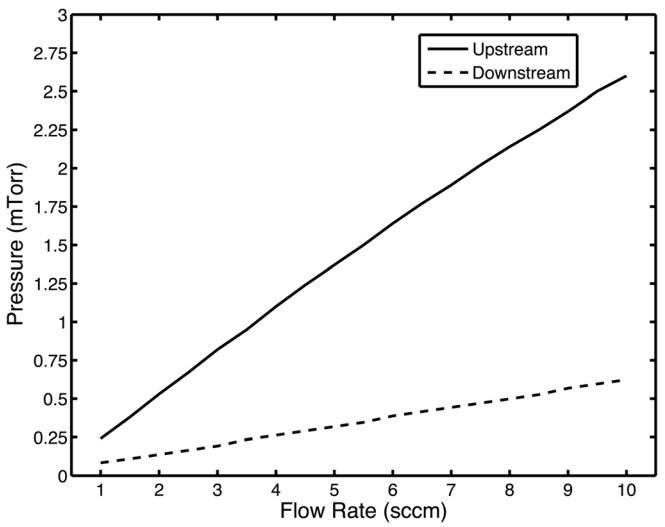

FIG. 2. Pressure vs. flow rate measured at the upstream and downstream endplates.

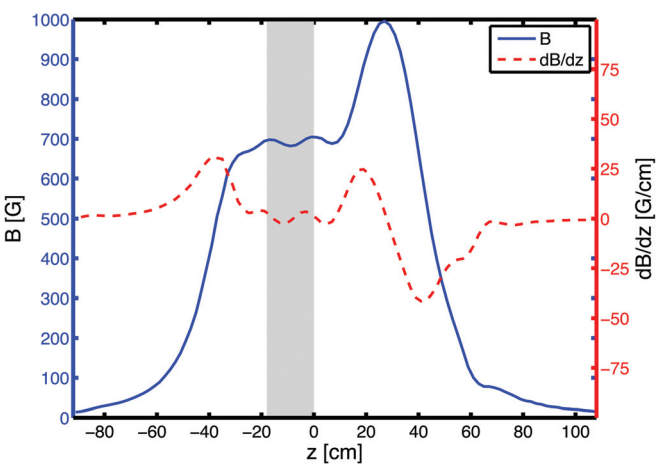

FIG. 3. (Color online) Axial magnetic field (B_z) and magnetic field gradient (dB_z/dz) vs. z for magnet current I = 60 A. The solid line denotes B_z and the dashed line denotes dB_z/dz. The shaded region shows the extent of the rf antenna. The chamber outline is shown for reference.

III. DIAGNOSTICS

A. Retarding potential analyzers

Two RPAs are used to measure the ion energy distribution as a function of source parameters. The first, a two-grid (plus collector) design,[30] is used as the main diagnostic for the ion beam due to its small size (12 mm diameter, 6.6 mm aperture, and 22 mm long), which minimizes perturbations of the plasma when moved axially, especially in the 10 cm diameter source tube region. A second, larger, 50 mm diameter four-grid (plus collector) RPA, of a tested design used in Hall thruster research,[31,32] is used to verify the measurements of the first RPA in a region well away from the plasma source. The RPAs cannot be used simultaneously; therefore, the vacuum must be turned off and on between measurements. However, extensive operation of this source has shown the plasma characteristics are highly repeatable for a given set of experimental conditions.

For both RPAs, the measured collector current is sampled at 1 MS/s. The collector current is numerically differentiated then smoothed using a moving average (window is 0.3% of trace) and normalized if required for analysis. The derivative of the collector current is actually the energy distribution of the ions falling through the potential drop in front of the RPA but is often called the ion energy distribution function (IEDF).[4] In this work, the abbreviation "IEDF" refers to the differentiated collector current. One or the sum of two Gaussian distributions is fitted to the resulting IEDF in some cases, where noise is high.

1. Two-grid RPA

The first RPA, shown in Fig. 4, has two grids and a collector. The brass body of the RPA is 12 mm in diameter and 22 mm long, and a brass plug forms an aperture, 6.6 mm in diameter, at the entrance of the RPA. The plasma-facing grid is floating, insulated from the other grid and body using mica rings. The discriminator grid is biased with an insulated wire, passed through the inner mica body, which is forced against the discriminator grid holding ring. The copper collector is biased with a second wire passed through the rear of the RPA body. Both grids (discriminator and floating) are an electroformed nickel mesh, with a 60% transmission factor and 50.8 μm wire spacing (500 wires per inch).

The discriminator grid is biased with a Kepco BOP-500M supply, swept between 0 and 300 V. The collector is biased at −9 V using a battery, and the collector current is measured through a 150 kΩ resistor to chamber ground. An AD620 instrumentation amplifier at unity gain (10 GΩ input impedance) is used to measure the voltage drop across the resistor. A digital storage oscilloscope records both the discriminator voltage and the voltage across the current-measurement resistor. An HP 33120A signal generator is used to sweep the discriminator supply at 3 Hz, and the recorded waveform is averaged a minimum of 60 times.

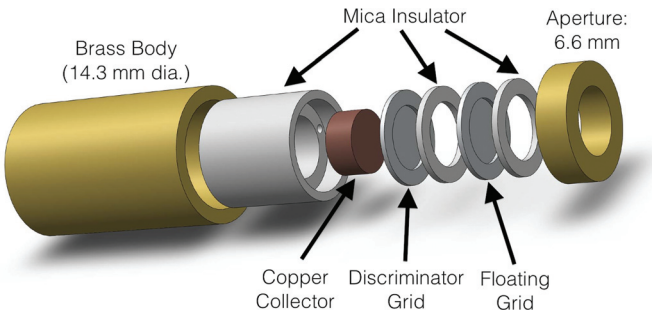

FIG. 4. (Color online) Two-grid RPA construction.

The RPA is attached and the body is electrically grounded to a 1/4″ stainless steel probe shaft which enters the system through the downstream endplate at $r=6$ cm. Two 90-degree bends in the probe shaft, 5 cm from the front face of the RPA, align the RPA on-axis at $r=0$ cm. This RPA can be swept axially from $z=50$ cm to $z=80$ cm.

2. Four-grid RPA

A four-grid (plus collector) RPA, used in Hall Thruster research,[31,32] was used to validate the results of the two-grid RPA. The four-grid RPA is much larger (50 mm diameter); therefore, it cannot be used axially along the entire system due to its size limitations and increased plasma perturbation.

The four grids are a plasma-facing grid, an electron repeller, the ion discriminator, and a secondary electron repeller. The grid voltages are tuned to provide the best raw current trace, such that the collector current approaches zero for high bias voltages and the collector current saturates at low bias voltages. The plasma-facing grid is floated, the electron repeller is biased at −120 V, the ion discriminator is swept from 0 to 300 V (using the Kepco BOP-500M supply), and the secondary electron repeller is biased at −83 V via a 9 V battery from the collector.[33] The collector is biased at −74 V with a high voltage battery, and the current is measured through a 150 kΩ resistor to chamber ground, again with an AD620 instrumentation amplifier.

B. Emissive probe

A floating emissive probe is used to measure the plasma potential, which has been shown to be appropriate in sources similar to ours.[22] A thoriated tungsten filament, 25 μm in diameter and 6.8 mm long, is spot-welded between two 3 cm long gold-plated nickel wires coated entirely in Sauereisen No. 31 ceramic cement. The last 40 cm (to the tungsten filament) of the probe shaft is coated in the insulating ceramic cement to minimize the effect of the grounded stainless steel probe shaft on the system. The probe enters the system through the downstream endplate, and a 90-degree bend at then end of the probe shaft puts the filament on-axis ($r=0$ cm) in the system, oriented perpendicular to the B field.

A Fluke 179 DMM, with an input impedance >10 MΩ, is used to measure the floating potential of the emissive probe in steady-state. An HP isolated DC supply supplies the filament current, which is increased until the measured floating potential saturates. For a 25 μm filament, the required filament heating current is around 210 mA.

C. Single and double probes

Our planar double probe is constructed from two 2.4 mm tantalum discs spot-welded to gold plated nickel wires, spaced 6 mm apart. The probes are coated with Sauereisen No. 31 cement except for the front-facing surfaces of the discs (facing the gas flow—z direction). The front-facing surfaces of the probes are aligned such that the normal to the probe surface is parallel to B_z. The probe can be used as a single probe with only one disc biased with respect to ground, or as a double probe, with the discs biased relative to each other but electrically isolated from ground. A single probe similar to this was used previously on this facility in earlier, high-pressure helicon experiments.[34]

The probes are biased using a custom-built double probe supply. A PA241 high voltage op-amp, powered by an isolated DC bipolar supply, amplifies the sweep signal, which is fed through an AD210 isolation amplifier to the op-amp. The probe current is measured through a resistor whose voltage drop is measured with another AD210 isolation amplifier. The probe voltage is measured through a high impedance voltage divider network with a third AD210 isolation amplifier. The supply can be used to drive a single probe by simply connecting one of the probe outputs (signal ground) to the stainless steel expansion chamber (earth ground).

When the probe is used as a single (Langmuir) probe, an rf choke is used to increase the probe's impedance at the rf drive frequency to avoid oscillations that can falsely increase the measured bulk electron temperature.[35] A parallel LC circuit, resonant at the rf frequency (13.56 MHz), is used with $Q = 15$.

The ion density is calculated from the ion saturation current by fitting to the ion saturation portion of the curve, subtracting the linear increase from sheath expansion, and using[36]

$$n_e = \frac{I_{sat}}{0.6eA_s\sqrt{\frac{T_e}{M_{Ar}}}}, \tag{1}$$

where I_{sat} is the ion saturation current, e is the elemental charge, A_s is the physical probe area, T_e is the electron temperature, and M_{Ar} is the mass of argon. Bulk electron temperatures are extracted from the single probe data near the floating potential by fitting an straight line to the logarithm of the electron current (after the ion saturation current has been subtracted, up to the plasma potential).

The double probe current traces are fitted to a hyperbolic tangent plus a linear rise due to sheath expansion[37,38]

$$I(V) = I_{sat}\tanh\left(\frac{eV}{2kT_e}\right) + \frac{V}{S}, \tag{2}$$

where I_{sat} is the ion saturation current, e is the elemental charge, k is the Boltzmann constant, T_e is the electron temperature, and S is a sheath expansion factor. The ion saturation current, bulk electron temperature, and the sheath expansion factor are used as fitting parameters. It should be noted that a double probe samples the electron distribution at or near the floating potential,[37] and, therefore, the fitted electron temperature is at the floating potential and the fitting assumes a single Maxwellian distribution, which may not hold in our rf source at lower pressures.[27]

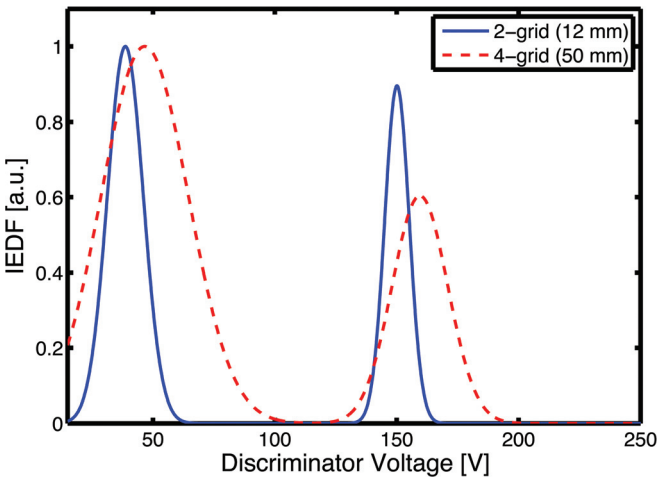

FIG. 5. (Color online) Comparison of 4-grid (red, dashed) and 2-grid RPA (blue, solid) measurements. Conditions are Q = 1.3 sccm, B = 340 G, P = 100 W.

IV. RESULTS

A. RPA validation

In order to validate the results of the 2-grid RPA, the 4-grid RPA was used for the same conditions and the measured IEDFs compared, which are shown in Fig. 5. The flow rate is 1.3 sccm, rf power is 100 W, and the magnetic field is 340 G in the source region. For this comparison, the analyzers' collectors were placed at the same z location (z = 64 cm) to provide the best comparison of the two RPAs. The grid spacing for the 4-grid RPA is larger than that of the 2-grid RPA, which meant the front-facing grids of the analyzers were offset by 5 cm. There is a slight difference between the measured potentials and widths of the bulk and the beam ions between the two analyzers; however, the beam energies (differences between the bulk and beam potentials) are within 10 V (10%). The differences between the RPAs could be due to spatial averaging, resulting from the larger grid area of the 4-grid RPA and the perturbation introduced by the 4-grid RPAs larger physical size. From the subsequent investigation of the beam characteristics, we have observed the 2-grid RPA provides the best agreement with the emissive probe data. For the rest of the experimental results shown, the smaller (12 mm diameter) 2-grid RPA is used.

In order to investigate rf perturbation effects on the 2-grid RPA, it was also installed into the helicon system with the plasma-facing grid facing the walls of the expansion chamber (perpendicular to the direction of the measured ion beam). The ion distribution function with the RPA in this configuration, for the same plasma conditions that produced an ion beam, was single-peaked (at the measured background, plasma potential) for all source parameters tested, indicating the negligible rf perturbation on the RPA. This is a common method used to verify that rf perturbations are not causing false beam indications.[10,24]

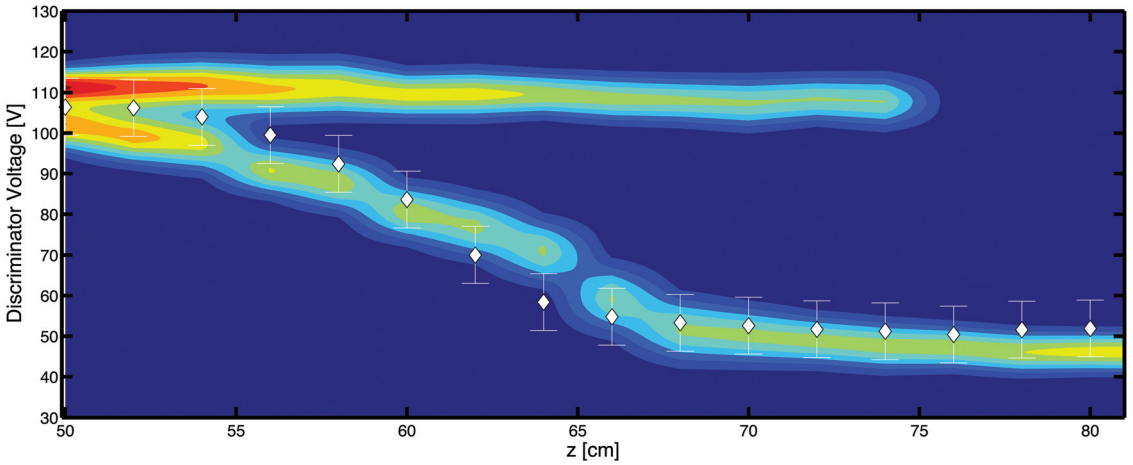

FIG. 6. (Color online) Ion energy distribution function from z = 50–80 cm measured by the 12 mm diameter RPA and fitted with one or two Gaussian distributions. The flow rate is 2 sccm, rf power is 100 W, and magnetic field in the source region is 340 G. Color (online) or gray-scale indicate the height of the distribution and the color map has been compressed in order to keep the data visible throughout the z domain. Floating emissive probe data are also shown (white diamonds).

B. Axial ion beam evolution

The axial dependence of the ion energy, electron density, and electron temperature were examined for source parameters that provide a well-defined ion beam population. The flow rate for this "test case" is 2 sccm (0.53 mTorr upstream and 0.16 mTorr downstream), the rf power is 100 W, and the magnetic field is 340 G in the source region. Figure 6 shows the RPA-measured, Gaussian-fitted ion energy distribution as a function of axial distance, with color (online) or gray-scale indicating the height of the distribution. The color/gray-scale map has been compressed to keep the data visible throughout the z domain due to the large spatial variation of the ion density (see Fig. 7 below, a factor of 36). The observed beam-ion potential (relative to chamber ground) is 110 V, and the bulk-ion potential varies from 110 V to 45 V as the RPA is moved axially over 25 cm into the expansion chamber. The ion beam energy is equal to the difference between the beam ion potential and the plasma potential ($E_b = e[V_{beam} - V_{plasma}]$), and increases from the bulk, background flow around $z = 45$ cm (slightly upstream of the minimum z position of the RPA) up to 65 eV at $z = 65$ cm. The beam density decreases into the expansion chamber due to expansion and ion-neutral charge-exchange collisions, and the beam decays over its 25 cm axial extent and vanishes by $z = 78$ cm as the fast ions collide with neutrals and produce slow (thermal) ions. The plasma potential is measured with the floating emissive probe for the same conditions and is also shown in Fig. 6 as white diamonds. This plasma potential agrees well with potential of the bulk population of ions measured by the RPA.

The plasma density and bulk electron temperature are shown in Fig. 7 for the same spatial domain and source conditions in Fig. 6. The electron density, measured with the single (Langmuir) probe biased in ion saturation, decreases rapidly through the ion acceleration region ($z = 50$ cm to $z = 65$ cm) from 8.8×10^9 cm^{-3} to 2.4×10^8 cm^{-3} (a factor of ~36) from $z = 50$ cm to $z = 65$ cm and then rises slowly to 7×10^8 cm^{-3} from $z = 65$ cm to $z = 80$ cm. The bulk electron temperatures obtained from both the single and double probes, which show good agreement, show a rise from 6 eV upstream of the ion acceleration region to 9 eV just downstream of the ion acceleration region in the expansion chamber.

The unfitted ion energy distribution, from the small RPA, as the plasma flows into the expansion chamber is shown in Fig. 8 for a flow rate of 4 sccm, 100 W rf power, and 670 G magnetic field. The higher flow rate (pressure) and magnetic field than for the data shown in Figs. 6 and 7 result in a lower energy beam with a shorter axial extent, which provides a full view of the evolution from a single-peaked distribution at $z = 50$ cm to a bimodal distribution and back to a single-peaked distribution at $z = 80$ cm. The peak in the upstream ($z < 60$ cm) distribution appears to increase slightly in energy as the RPA is moved downstream. However, as Byhring[8] noted, the distribution remains "inside" the initial distribution and the apparent increase appears because the lower energy ions in the beam are

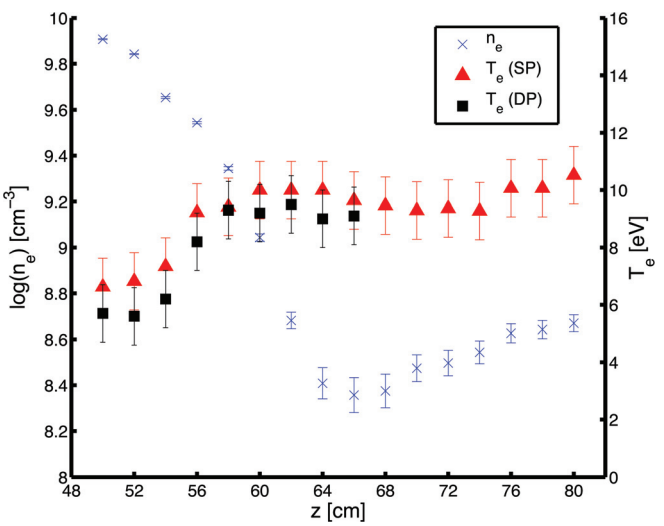

FIG. 7. (Color online) Electron density (single probe) and temperature measured with single and double probes for the same conditions and spatial domain shown in Fig. 6.

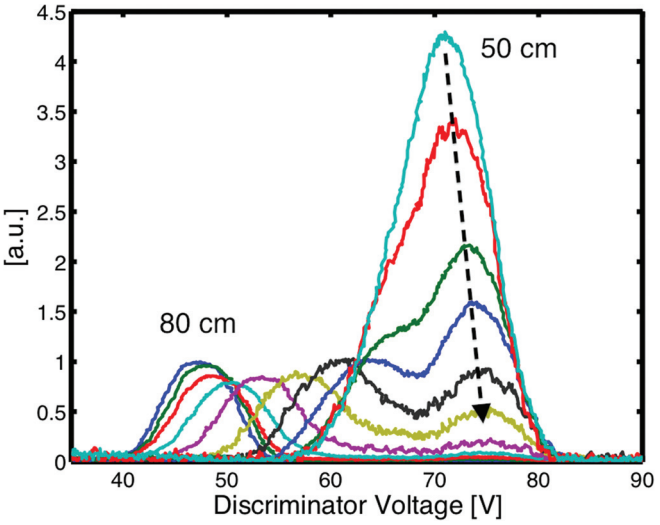

FIG. 8. (Color online) Detailed behavior of the ion energy distribution function measured with the 12 mm RPA from z = 50 to z = 80 cm for flow rate of 4 sccm, 100 W rf power, 670 G source magnetic field. The data shown are unfitted.

preferentially lost due to the energy dependence of the charge-exchange cross section.

C. Ion beam energy scaling

The parametric scaling of the ion beam energy is investigated, including variation with flow rate, rf power, and magnetic field strength.

1. Flow rate

Figure 9 shows the beam energy (difference between upstream plasma potential at $z = 50$ cm and the expansion chamber plasma potential at $z = 80$ cm) as a function of argon flow rate at $P_{rf} = 100$ W and B = 340 G. As flow rate is decreased, an increase in the beam energy is observed from 35 eV at 4 sccm to over 110 eV at 1.3 sccm. Below 1.3 sccm, the source becomes unstable[5] and steady state operation was not possible, with oscillations in visible light likely due to neutral starvation and replenishing as seen by Degeling[39] and previously on this source by Wiebold.[40]

2. Magnetic field strength

Figure 10 shows the behavior of the beam energy as a function of the source region magnetic field, for a flow rate Q = 2 sccm and $P_{rf} = 100$ W. The beam energy has been extracted from individual z scans with the 2-grid RPA. The beam energy can be represented as the difference between the upstream source potential and the downstream chamber potential as measured by the RPA. The measured beam energy shown in Fig. 10 is then independent of the z position and extent of the acceleration region, since the data are not taken at a single z location. The beam energy monotonically decreases with increasing magnetic field, from 65 eV at 340 G to 27 eV at 1000 G. Also shown in Fig. 10 is the z extent of the acceleration region, which decreases in length and moves further into the expansion chamber with increasing magnetic field.

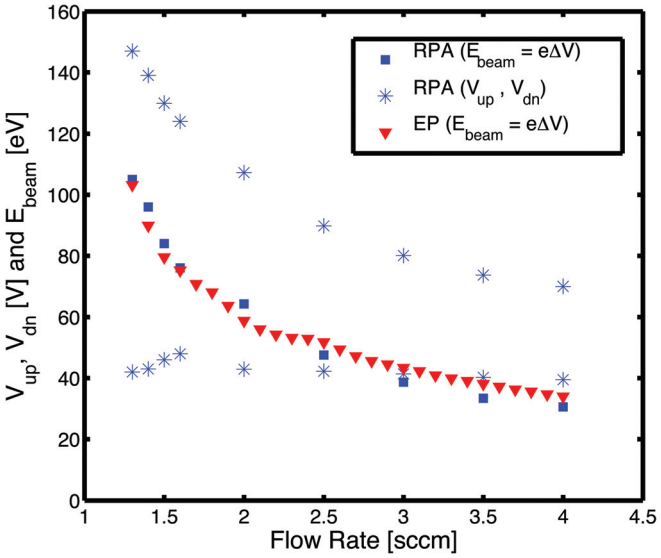

FIG. 9. (Color online) Ion beam energy (E_{beam}) and upstream and downstream potentials (V_{up}, V_{dn}) vs. flow rate for 100 W rf power and 340 G magnetic field. The stars represent the higher, upstream (z = 50 cm) and lower, downstream (z = 80 cm) potentials measured with the 2-grid RPA. The beam energy is calculated using the difference between the upstream and downstream potentials as measured by both the small (2-grid) RPA (squares) and emissive probe (triangles). Error bars are not shown for clarity.

3. Rf power

The ion beam energy was also measured as a function of the rf coupled power. For each power level, the reflected power measured with the directional coupler was minimized (<5%). Figure 11 shows the ion beam energy ($E_b = e[V_{beam} - V_{plasma}]$) at $z = 64$ cm as a function of rf input power for a flow rate of 1.3 sccm and magnetic field of 340 G in the source region. The smaller RPA was not used here out of concern for its fragile grids. Instead, the more robust, larger 4-grid RPA was used. The ion beam energy increases

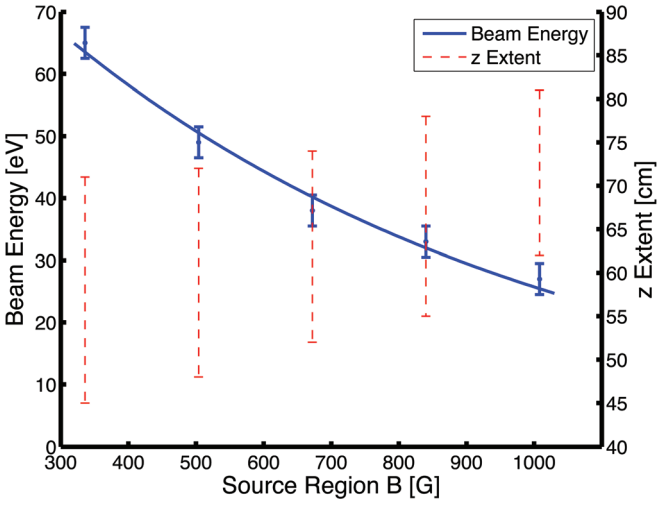

FIG. 10. (Color online) Beam energy ($E_b = e[V_{beam} - V_{plasma}]$) vs. source region magnetic field value (field profile does not change) for flow rate Q = 2 sccm, rf power P = 100 W, and location z = 64 cm. Also shown is the z extent (cm) of the DL structure taken from individual axial scans of the ion distribution.

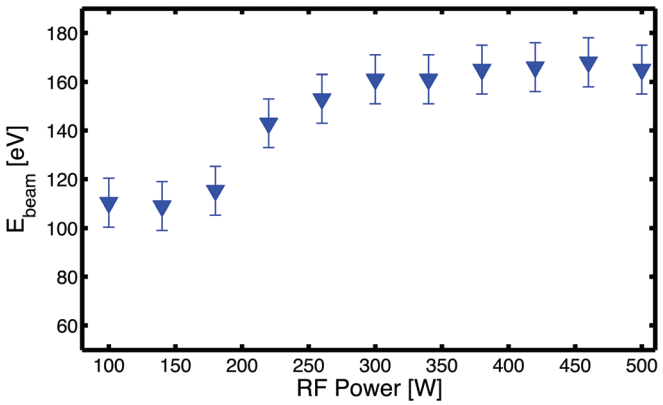

FIG. 11. (Color online) Ion beam energy as measured with the 4-grid RPA vs. rf power at 1.3 sccm flow rate and 340 G source-region magnetic field at z = 64 cm.

from 110 eV at 1.3 sccm, in agreement with the two-grid RPA data shown in Fig. 9, to 165 eV at $P_{rf} = 500$ W.

V. DISCUSSION

In the MadHeX system, substantial potential drops (up to 165 V) over several centimeters lead to the formation of high-energy ion beams. The potential profile for 2 sccm flow rate, 100 W rf power, and 340 G source magnetic field shows a drop of 65 V over 20 cm, which is much larger than that predicted by simple Boltzmann plasma expansion

$$V(z) = V_0 + \frac{kT_e}{e}\ln\left(\frac{n(z)}{n_0}\right), \tag{3}$$

where V_0 is the upstream potential, T_e is the electron temperature (assumed constant through the expansion), n_o is the upstream electron density, and $n(z)$ is the electron density as a function of z. As shown in Fig. 7 for Q = 2 sccm, the electron density decrease over the region of the potential drop is about 36, therefore, to attain a 65 V potential drop via Boltzmann expansion, an electron temperature of over 18 eV would be required, well above our measured bulk electron temperatures of 6 eV as one approaches the acceleration region. This potential structure has the characteristics of a CFDL as seen in other experiments.[41]

It should be noted that the neutral pressure gradient that exists in the system is not a significant source of the measured ion acceleration. The Knudsen number, which relates the argon neutral-neutral mean free path to the chamber diameter, is given by

$$\mathrm{Kn} = \frac{\lambda_{\mathrm{mfp}}}{D} = \frac{1}{\sqrt{2}D\pi d_o^2 n_g}, \tag{4}$$

where D is the characteristic dimension of the system, d_0 is the hard-sphere diameter of argon, and n_g is the gas density.[42] For the pressures measured in our system, the Knudsen number $\mathrm{Kn} \gtrsim 1$, such that the flow is approaching free-molecular. The average neutral velocity in free-molecular flow $v_{av} = \sqrt{\frac{8kT}{\pi M_{Ar}}}$ is the characteristic velocity of the flow, which for room temperature is ~400 m/s. If there is neutral heating during the source operation such that the neutrals are in thermal equilibrium with the plasma ions [roughly 0.1 eV (Ref. 43)], $v_{av} \sim 800$m/s. The measured ion beam velocities are in the range of 13–28 km/s; therefore, the background neutral velocities are much smaller than the ion beam velocities, even accounting for this neutral heating.

For the source parameters shown in Fig. 6, the Debye length (λ_D) increases from 0.2 mm to 1.5 mm through the ion acceleration region from $z = 48$ cm to $z = 68$ cm. Therefore, the 20-centimeter-long ion acceleration region is between $L_{DL} = 13$–$100\ \lambda_D$ long, on the order of the spatial extent of other double layers measured in expanding helicon plasmas.[6]

Double layers in a system with entirely electrically conducting walls are limited to a potential drop of 3–5kT_e in argon due to the requirement that there be a nonzero sheath potential drop at the walls throughout the system[16]

$$\frac{eV_p - eV_{fl}}{kT_e} = \frac{1}{2}\left[1 + \ln\left(\frac{M_{Ar}}{2\pi m}\right)\right] \sim 5.2, \tag{5}$$

where M_{Ar} is the argon mass and m is the electron mass. However, in the MadHeX system and others',[8–10] with an insulating source and grounded expansion chamber, ion beam energies exceed the typical 3–5kT_e and can be well over 10kT_e. In our system at 2 sccm at 100 W rf power, the DL potential drop is 13kT_e, using the measured upstream bulk electron temperature.[27] In order to support these larger potential drops, there is likely some positive charging of the insulating Pyrex wall occurring in the upstream, source region as reported by others.[2,44–48] The upstream plasma potential in our system is well over 100 V as measured with both the RPA and emissive probes, much larger than the $eV_p \sim 5.2kT_e$ for grounded walls like the potentials measured in the expansion chamber. This Pyrex wall charging leads to a higher plasma potential upstream of the ion beam formation region and, therefore, a larger potential drop and higher energy ion beams.

The increase in bulk electron temperature through the double layer is the result of the high potential barrier electrons face on the source side of the DL as they travel downstream. Takahashi[27] has measured a depleted two-temperature Maxwellian distribution in the central region upstream of the DL in their system, with an 8–10 eV bulk and a 4–5 eV tail distribution. The electrons that are energetic enough to make it over the DL potential drop are in the tail of the distribution, and the measured downstream electron distribution only contains the 4–5 eV distribution from the upstream tail. In our system, we see *higher* electron temperatures downstream, suggesting we may have a two-temperature Maxwellian distribution upstream, with a tail temperature that is hotter than the bulk, as seen by Cohen,[19] and there is a theoretical evidence that non-Maxwellian electron distributions are required for the formation of double layers.[18]

The ion beam decays mainly due to ion-neutral charge-exchange (CX) collisions. The mean free path for these interactions is given by

$$\lambda_{cx} = \frac{1}{n_g \sigma_{cx}}, \tag{6}$$

where $n_g[\mathrm{cm}^{-3}] = 3.25 \times 10^{13}\ p[\mathrm{mTorr}]$ and σ_{cx} is the total ion collisional cross section and is a function of the incident argon ion energy. The cross section σ_{cx} varies from 8×10^{-15} cm^2 at low ($E_i < 4$ eV) energies and decreases to 4×10^{-15} cm^2 at higher ($E_i > 300$ eV) energies.[36] For 65 eV ions measured at 2 sccm (0.4 mTorr in the ion acceleration region) shown in Fig. 6, $\sigma_{cx} \sim 5 \times 10^{-15}$ cm^2 which results in a mean free path $\lambda_{cx} \sim 15$ cm. Since the mean free path is the 1/e length for the beam decay, the beam is decaying slightly faster than the rate predicted by the mean free path calculation. However, the pressure in the ion acceleration region is only an estimate, and the beam ions' energy is not a constant 65 eV throughout the DL; therefore, the cross section used in the above calculation is a lower bound and the mean free path calculated is an upper bound. The electron-neutral cross section σ_{en} is much smaller than σ_{cx}, roughly $3\text{–}8 \times 10^{-16}$ cm^2 for $kT_e \sim 5\text{–}8$ eV (Ref. 49) therefore, the electron-neutral mean free path $\lambda_{en} \geq 90$cm is substantially longer than λ_{cx}, hence, the ion acceleration region (and most of the system) is electron-neutral collisionless.

Due to the low electron-neutral collisionality, the slight increase in electron density downstream of the acceleration region ($z = 64$ cm to $z = 80$ cm) seen in the axial scan in Fig. 7 is likely not due to ionization. The rise likely occurs due to the slowing of ions in the beam from charge-exchange collisions. The fast ions become slow ions (producing fast neutrals) and the electrons, assuming quasineutrality, also slow down, and their density increases slightly. The density remains lower and does not return to its value upstream of the double layer, because the plasma is expanding along the magnetic field lines, and there are losses through the expansion region as well as some reflected electrons on the high-potential side of the double layer region.

The fraction of the ions in the beam can be calculated from the collected RPA current at different discriminator voltages. The collected current goes as[3]

$$I_{\mathrm{RPA}} \sim e A_{\mathrm{RPA}} T^2 n_i v_i, \tag{7}$$

where e is the fundamental charge, A_{RPA} is the RPA collection area, T is the grid transmission factor, n_i is the ion density, and v_i is the ion velocity at the collector. The ion density and velocity are dependent on the discriminator voltage and can be divided into the beam and bulk ions. The bulk ions fall into the collector with at least the Bohm velocity (c_s) and the beam ions approach the collector on average at the beam velocity, v_{beam}. The ion current in the bulk and beam distributions can be calculated from either the raw collected current or the fits to the IEDF. Using the fits, it is possible to extract the portions of the collected current from the beam and bulk ions. The fraction of the ions in the beam is then

$$\frac{n_{\mathrm{beam}}}{n_{\mathrm{bulk}} + n_{\mathrm{beam}}} = \frac{\frac{I_{\mathrm{beam}}}{v_{\mathrm{beam}}}}{\frac{I_{\mathrm{bulk}}}{c_s} + \frac{I_{\mathrm{beam}}}{v_{\mathrm{beam}}}}, \tag{8}$$

where n_{beam} is the beam ion density, n_{bulk} is the bulk ion density, c_s is the ion sound speed calculated using the measured electron temperature from the single probe, v_{beam} is the beam velocity, and I_{beam} and I_{bulk} denote the currents collected by the 2-grid RPA for the beam and the bulk distributions, respectively, calculated from the integrated fits to the IEDF. The constants e, A_{RPA}, and T in Eq. (7) cancel from the beam fraction calculation. For 2 sccm at 100 W and 340 G, the calculated beam fraction is ~50% at z = 62 cm, and for 1.3 sccm at 100 W and 340 G, the beam fraction is ~60%, also at z = 62 cm.

The behavior of the beam energy with flow rate, magnetic field, and rf power is dominated by the effect of each respective parameter on the operation of the source upstream. The plasma potential in the source is strongly affected by changes in these parameters, while the plasma potential in the downstream expansion chamber remains relatively constant,[5] ranging from 40 to 50 V for all conditions investigated (roughly $\sim 5kT_e$), as shown in Fig. 9. The upstream, source potential is highest for low magnetic fields, low flow rates, and high powers. The highest beam energy is achieved when these parameters are adjusted so the upstream potential is highest, but the source operation is still stable. At very low flow rates, the source is starved for neutrals and the region of visible light output shifts, and there is no longer a signal observed by the RPAs. For very low magnetic fields, there is also a noticeable "jump" in the operation of the source for $B \leq 300$ G and the beam disappears on the RPAs. The floating emissive probe continues to show an increase in upstream potential, but the downstream density is too low to measure a beam on the RPA. Higher power operation also leads to higher beam energies in our investigation up to $P_{\mathrm{rf}} = 500$ W.

As the magnetic field is increased, the DL structure shifts further into the expansion chamber. The axial extent of the DL decreases slightly, as expected since the DL is a phenomenon dependent on the Debye length, a function of the electron density and temperature, which are affected by the magnetic field value in the source region. Single probe data reveal that the electron density increases by a factor of ~2.5 and the bulk electron temperature decreases slightly (~1 eV) as B increases from 340G - 1000G, resulting in a shorter Debye length (at a given z location) and axial extent of the DL.

VI. CONCLUSION

Ion beams up to $E_b = 165$ eV are observed in argon at 500 W rf power in our expanding helicon system with a half-turn double-helix antenna, a magnetic nozzle, and an expansion chamber. The measured potential drop, using both a floating emissive probe and RPA, is larger than that predicted by simple Boltzmann plasma expansion. Electron density and temperature measurements show that the ion acceleration region is less than 100 Debye lengths long; therefore, we can conclude that the ion acceleration in our system is due to a double layer that forms near the region of physical expansion. The spatial extent and variation of the ion beam, electron bulk temperature, and plasma density are examined in detail through the acceleration and expansion

regions. The large potential variation arising from the DL (65 V at 2 sccm) results in a substantial density drop through the DL by a factor of 36, and the bulk electron temperatures range from 6 to 9 eV with higher temperatures measured downstream of the double layer. A substantial ion beam (165 eV) forms with 500 W rf power coupled, likely a result of wall charging upstream in the source. Parameter changes (flow rate, magnetic field and rf power) result in changes in the upstream source potential while the downstream expansion chamber potential changes relatively little.

ACKNOWLEDGMENTS

We thank Professor Wong of Nonlinear Ion Dynamics, LLC, and UCLA for fabrication of the 2-grid RPA, Professor Walker of Georgia Institute of Technology for insightful discussion and fabricating the 4-grid RPA, and Professor Hershkowitz and Chi-Shung Yip of UW-Madison for assistance in fabrication of the emissive and tantalum probes. Research supported by AFOSR Grant No. FA9550-10-1-0396 and in part by AFOSR Grant No. FA9550-09-1-0357.

[1]S. A. Cohen, N. S. Siefert, S. Stange, R. F. Boivin, E. E. Scime, and F. M. Levinton, Phys. Plasmas **10**, 2593 (2003).
[2]C. Charles and R. W. Boswell, Appl. Phys. Lett. **82**, 1356 (2003).
[3]C. Charles and R. W. Boswell, Phys. Plasmas **11**, 1706 (2004).
[4]C. Charles and R. W. Boswell, Phys. Plasmas **11**, 3808 (2004).
[5]C. Charles, Phys. Plasmas **12**, 044508 (2005).
[6]X. Sun, A. M. Keesee, C. Biloiu, E. E. Scime, A. Meige, C. Charles, and R. W. Boswell, Phys. Rev. Lett. **95**, 025004 (2005).
[7]J. Prager, R. Winglee, T. Ziemba, B. Race Roberson, and G. Quetin, Plasma Sources Sci. Technol. **17**, 025003 (12 p.) (2008).
[8]H. S. Byhring, C. Charles, A. Fredriksen, and R. W. Boswell, Phys. Plasmas **15**, 102113 (2008).
[9]V. F. Virko, Y. V. Virko, V. M. Slobodyan, and K. P. Shamrai, Plasma Sources Sci. Technol. **19**, 015004 (2010).
[10]A. Fredriksen, L. N. Mishra, and H. S. Byhring, Plasma Sources Sci. Technol. **19**, 034009 (2010).
[11]E. E. Scime, I. A. Biloiu, Jr., J. Carr, S. Chakraborty Thakur, M. Galante, A. Hansen, S. Houshmandyar, A. M. Keesee, D. McCarren, S. Sears, C. Biloiu, and X. Sun, Phys. Plasmas **17**, 055701 (2010).
[12]N. Plihon, P. Chabert, and C. S. Corr, Phys. Plasmas **14**, 013506 (2007).
[13]N. Hershkowitz, Space Sci. Rev. **41**, 351 (1985), ISSN 0038-6308, 10.1007/BF00190655.
[14]M. A. Raadu, Phys. Rep. **178**, 25 (1989), ISSN 0370-1573.
[15]C Charles, Plasma Sources Sci. Technol. **16**, R1 (2007).
[16]F. F. Chen, Phys. Plasmas **13**, 034502 (2006).
[17]M. A. Lieberman and C. Charles, Phys. Rev. Lett. **97**, 045003 (2006).
[18]E. Ahedo and M. Martínez Sánchez, Phys. Rev. Lett. **103**, 135002 (2009).
[19]S. A. Cohen, X. Sun, N. M. Ferraro, E. E. Scime, M. Miah, S. Stange, N. S. Siefert, and R. F. Boivin, IEEE Trans. Plasma Sci. **34**, 792 (2006), ISSN 0093-3813.
[20]O. Sutherland, C. Charles, N. Plihon, and R. W. Boswell, Phys. Rev. Lett. **95**, 205002 (2005).
[21]S. Chakraborty Thakur, Z. Harvey, I. A. Biloiu, A. Hansen, R. A. Hardin, W. S. Przybysz, and E. E. Scime, Phys. Rev. Lett. **102**, 035004 (2009).
[22]T. Lafleur, C. Charles, and R. W. Boswell, Phys. Plasmas **16**, 044510 (2009).
[23]J. Ling, M. D. West, T. Lafleur, C. Charles, and R. W. Boswell, J. Phys. D: Appl. Phys. **43**, 305203 (2010).
[24]T. Lafleur, C. Charles, and R. W. Boswell, Phys. Plasmas **17**, 043505 (2010).
[25]K. Takahashi, C. Charles, R. W. Boswell, and T. Fujiwara, Appl. Phys. Lett. **97**, 141503 (2010).
[26]K. Takahashi, C. Charles, R. W. Boswell, and R. Hatakeyama, Phys. Plasmas **15**, 074505 (2008).
[27]K. Takahashi, C. Charles, R. W. Boswell, T. Kaneko, and R. Hatakeyama, Phys. Plasmas **14**, 114503 (2007).
[28]C. M. Denning, M. Wiebold, and J. E. Scharer, Phys. Plasmas **15**, 072115 (2008).
[29]S. M. Tysk, C. M. Denning, J. E. Scharer, and K. Akhtar, Phys. Plasmas **11**, 878 (2004).
[30]A. Y. Wong, *Introduction to Experimental Plasma Physics* (University of California, Los Angeles, USA, 1977).
[31]B. E. Beal, "Clustering of Hall effect thrusters for high-power electric propulsion applications," Ph.D. thesis (The University of Michigan, 2004).
[32]D. L. Brown, "Investigation of low discharge voltage Hall thruster characteristics and evaluation of loss mechanisms," Ph.D. thesis (The University of Michigan, 2009).
[33]G. D. Conway, A. J. Perry, and R. W. Boswell, Plasma Sources Sci. Technol. **7**, 337 (1998).
[34]X. M. Guo, J. Scharer, Y. Mouzouris, and L. Louis, Phys. Plasmas **6**, 3400 (1999).
[35]O. Auciello and D. L. Flamm, *Plasma Diagnostics: Discharge Parameters and Chemistry* (Academic, 1989), Vol. 1.
[36]M. A. Lieberman and A. J. Lichtenberg, *Principles of Plasma Discharges and Materials Processing*, 2nd ed. (Wiley, Hoboken, New Jersey, 2005).
[37]Y.-c. Ghim(Kim) and N. Hershkowitz, Rev. Sci. Instrum. **80**, 033502 (2009).
[38]E. O. Johnson and L. Malter, Phys. Rev. **80**, 58 (1950).
[39]A. W. Degeling, T. E. Sheridan, and R. W. Boswell, Phys. Plasmas **6**, 1641 (1999).
[40]M. Wiebold, H. Ren, C. M. Denning, and J. E. Scharer, IEEE Trans. Plasma Sci. **37**, 2110 (2009), ISSN 0093-3813.
[41]K. Takahashi, C. Charles, R. Boswell, and R. Hatakeyama, Phys. Plasmas **15**, 074505 (2008).
[42]J. O'Hanlon, *A User's Guide to Vacuum Technology*, 3rd ed. (Wiley, Hoboken, New Jersey, 2003).
[43]R. F. Boivin and E. E. Scime, Rev. Sci. Instrum. **74**, 4352 (2003).
[44]C. Charles, J. Vac. Sci. Technol. A **20**, 1275 (2002).
[45]C. Charles and R. W. Boswell, J. Vac. Sci. Technol. A **13**, 2067 (1995).
[46]C. Charles, J. Phys. D: Appl. Phys. **42**, 163001 (2009).
[47]A. Dunaevsky, Y. Raitses, and N. J. Fisch, Appl. Phys. Lett. **88**, 251502 (2006).
[48]A. Meige, R. W. Boswell, C. Charles, and M. M. Turner, Phys. Plasmas **12**, 052317 (2005).
[49]A. Zecca, G. P. Karwasz, and R. S. Brusa, Riv. Nuovo Cimento **19**, 1 (1996), ISSN 0393-697X.